NASA CR-112360

Studies of Engine-Airframe Integrated Hypersonic Vehicles+

by

Heywood Salandy, Herbert Fox** and Walter Hoydysh***

New York University
Bronx, New York

Abstract

A parametric study of an integrated airframe and engine is presented for a hypersonic transport at an altitude of 70,000 feet and a free stream Mach number of 6. The engine considered is a subsonic combustion ramjet using conventional hydrocarbon fuels. The lift-to-drag ratio of the aircraft for two configurations, one with full capture and accelerated flight and the other allowing spillage of the leading shock and in unaccelerated flight, is studied. The parameters varied are the engine efficiencies, the angle of attack, the combustion rates, as well as the captured mass flow. Lift-to-drag ratios on the order of 6.5 are obtained.

+ The research was partially supported by the National Aeronautics and Space Administration under Grant NGR 33-016-131. The authors gratefully acknowledge the assistance of Prof. Antonio Ferri throughout the course of this investigation. We also thank Mr. Kirkham of NASA Langley Field for many useful suggestions and criticisms of the work presented here.

* Assistant Research Scientist
** Associate Professor of Aeronautics and Astronautics
*** Senior Research Scientist

Nomenclature

A	area
b	profile depth
D	drag
f	fuel-to-air ratio
h	altitude
I	impulse function
L	lift
ℓ	length of flat plate
M	Mach number
$\dot{m}$	mass flow
p	pressure
R	gas constant
R_e	Reynold's number
T	temperature; thrust
U	velocity
W	weight
α	angle of attack
γ	ratio of specific heats
δ	leading edge wedge angle
η_n	nozzle adiabatic efficiency
θ	slipstream angle
μ	viscosity
ρ	density
ϕ	fuel equivalence ratio
ω	inclination of thrust

Subscripts and superscripts

a	conditions at entrance of inlet
e	conditions at nozzle exhaust
0	stagnation conditions
2	conditions at inlet exit
4	conditions at combustion chamber exit
*	sonic conditions

1. Introduction.

With the advent of the supersonic transport attention is now being turned to the study of hypersonic vehicles for a variety of missions. These include for example, recoverable boosters and commercial transports with extended range on the order of 6000 nautical miles. In Ref. 1-3 preliminary studies indicating conceivable configurations, their corresponding missions and necessary performance are discussed.

Several problems immediately arise in any such discussion. These are related to the questions of vehicle cooling at hypersonic speeds, associated sonic boom, engine performance over a wide operating range of Mach numbers and configuration possibilities. The present work is one phase of a general study of engine-airframe integration dealing in large part with these questions. It would seem pertinent here to make some very brief remarks concerning these areas as a suitable introduction to the research described in this report, and to place it in the proper perspective and context.

It is clear that at hypersonic speeds (Mach numbers between 4 and 5 or even 12) standard radiation cooling is simply not efficient enough unless a change in the metallurgical state-of-the-art is simultaneously accomplished. If it is necessary to work with present material technology active cooling schemes are then required [4]. To this end we must consider the possibilities of ablation cooling, transpiration cooling and slot injection. The details of mechanisms employing the first two have been well documented in recent years. It has always been felt that slot injection (parallel to the free stream) would not be sufficiently effective. Recent experiments [5] have indicated that indeed in hypersonic flows with their attendant boundary layer

thicknesses it is conceivable that this technique can be employed successfully. Thus it appears that an active cooling system may in fact be feasible. The design of typical systems are the subjects of another phase of the overall work and are presented elsewhere (see Refs. 6 and 7).

Sonic boom studies indicate a substantial and beneficial altitude effect. In the case of the supersonic transport, considerations have been made which require cruise at roughly 60,000 ft. For the studies in Refs. 1-3 the typical cruise condition is obtained at altitudes nearer to 120,000 ft. This may then imply, from overpressure considerations, that a hypersonic transport is more practical.

Engine performance over extremely varied inlet conditions has always seemed to require variable geometry configurations. Recent studies (see Refs. 8 and 9) show that with careful application of the process of thermal compression[10] the effects of variable geometry (i.e. variable capture area) can be obtained without the requisite machinery. Indeed in the results of the present analysis we will presume that such fluid dynamic behavior is possible in the design of the integrated vehicle we propose.

The question of configurations is the subject of the present report. It is clear that as the flight Mach number increases better integration of the airframe and power plant is required. The size of the capture area and the interaction problems between inlet and nozzle and vehicle body make it crucial to consider the engine as an integral part of the airplane rather than as an individual unit to be affixed to pods wherever it is most convenient. Without making adequate concession to this essential integration a proper assessment of the performance of a hypersonic transport cannot be made[3].

The actual computation presented here will be recognized as standard analyses of the components of the vehicle. However, what is novel is exactly the approach taken to integrate the engine and airframe into a single unit. The engine cycle selected for study is the subsonic combustion ramjet. Performance improvement can be obtained by selecting a supersonic combustion engine; here, however, we choose to use technology within the state-of-the-art. We will discuss the performance in terms of the lift-to-drag ratio and thrust of the engine. To provide simple tools for this preliminary design two dimensional flow fields are considered. However, as will be indicated later, many of the results are applicable to the more realistic three dimensional geometry when the principles of integration are employed.

2. Analysis

In this section the procedure used for the performance calculations of the engine configurations with and without spillage and the technique employed for the determination of the lift-to-drag ratio are briefly summarized.

A. Engine Calculation

In Fig. 1a a schematic diagram of a standard subsonic combustion ramjet engine is displayed. Free stream conditions are determined by selection of flight altitudes and upstream Mach numbers. We consider the individual engine components sequentially; it will be recognized that the analysis is standard and may be found e.g. in Ref. 11.

(i) Diffuser

A recovery factor for inlet, r_{in},

$$r_{in} = p_{02}/p_{0a} \qquad (1)$$

is assumed. Since the diffuser is taken to be adiabatic $T_{02}(=T_{0a})$ can be found and p_{02} determined from Eq.(1). In general, for subsonic combustion, M_2 will usually be small so that $T_2 \simeq T_{02}$, $p_2 \simeq p_{02}$ and $c_{p2}(T_2)$ and $\gamma_2(T_2)$ can be found in a first approximation. Additional remarks regarding the appropriate selection of r_{in} may be found below in connection with correct charging of skin friction and shock losses to engine or airplane.

(ii) Combustion Chamber

Typical combustion studies yield the combustion temperature T_4 as a function of the inlet total temperature T_{02} and the fuel-to-air ratio, f, or equivalence ratio, $\Phi = (f/0.0667)$ for typical hydrocarbons. With f assumed and T_{02} computed as above, $T_4(f,T_{02})$ and $\gamma(f,T_{02})$ can be determined. For the present study it was assumed sufficient to take curve fits of the combustion data available in Ref. 12 and summarized in Fig. 2. For the analysis presented here, typical pressures require that the highest pressure available be used; the small variation with pressure indicated in Fig. 2 suggests this to be a reasonable assumption.

The remaining properties in the combustor are determined by assuming that it is a constant area duct and is choked at its exit. Then (see e.g. Ref. 13) since:

$$T_{04}/T_4 = (\gamma_4+1)/2 \tag{2}$$

$$2M_2^2(1+\gamma_4)\left\{1+[(\gamma_2-1)/2]M_2^2\right\}(R_4/R_2)(\gamma_2/\gamma_4)(1+\gamma_2 M_2^2)^{-2} = T_{02}/T_{04} \tag{3}$$

Eqs. (2) and (3) yield T_{04} and M_2+. The stagnation and static pressures and the throat area may be found from

$$p_{02}/p_{04} = (1+\gamma_4)[1+(\gamma_2-1)M_2^2/2]^{\gamma_2/(\gamma_2-1)} \div (1+\gamma_2 M_2^2)[(1+\gamma_4)/2]^{\gamma_4/(\gamma_4-1)} \tag{4}$$

+ Note that this provides a check on the approximation attendant to the diffuser exit.

$$p_{04}/p_4=(T_{04}/T_4)^{\gamma_4/(\gamma_4-1)} \tag{5}$$

$$A^* = [\dot{m}_a(1+f)/p_4]\ (R_4T_4/\gamma_4)^{\frac{1}{2}} \tag{6}$$

(iii) Nozzle

As in any nozzle design, one of two basic positions may be taken. We can assume that the flow is completely expanded so that $p_e=p_a$ and determine M_e, A_e/A^*, etc. On the other hand, it is conceivable that the area can be fixed in terms of A_e/A^* with M_e, p_e, etc. as results therefrom. Both techniques are employed here; the former will correspond to the full capture configurations while the latter to the balanced or spillage configuration. (See Figs. 1b and 1c) When the results for each are discussed, rationale for selection of the nozzle computation procedure will be provided; here we merely summarize the relations employed.

For this preliminary study it was deemed sufficient to take the specific heat constant in the nozzle. Then the nozzle adiabatic efficiency may be written as:

$$\eta_n=(T_{04}-T_e)\ /\ (T_{04}-T_{es}) \tag{7}$$

where T_{es} is the ideal exit static temperature.

Using this definition, the continuity, momentum and the energy equations yield expressions for area ratio, pressure ratio, and temperature ratio:

$$A_e/A^*=(1/M_e)\left\{(\gamma_4+1)/2[1+(\gamma_4-1)M_e^2/2]^{-1}\right\}^{\frac{1}{2}}\left\{[\eta_n-(\gamma_4-1)/(\gamma_4+1)]\right.$$
$$\left.\div\ (\eta_n-1+1/[1+(\gamma_4-1)M_e^2/2])\right\}^{\gamma_4/(\gamma_4-1)} \tag{8}$$

$$p_e/p_{04} = [\{ \eta_n - 1 + 1/[1+(\gamma_4-1)M_e^2/2]\} /\eta_n]^{\gamma_4/(\gamma_4-1)} \quad (9)$$

$$T_e/T_{04} = 1-\eta_n [1-(p_e/p_{04})^{(\gamma_4-1)/\gamma_4}] \quad (10)$$

Once M_e, T_e and p_e are determined, the exit density may be found from the equation of state and the exit velocity from the definition of Mach number.

(iv) Performance

The total thrust of the engine is the difference between the final and initial impulse of the air passing through the engine. The actual thrust then is that component of total thrust parallel to the free stream direction and the lift due to thrust is that component normal to the free stream direction. The impulse function, I, is simply defined as:

$$I = p_A + \rho U^2 A \quad (11a)$$

and therefore

$$T_{total} = I_e - I_a \quad (11b)$$

B. Aerodynamic Calculations.

Before proceeding to the computation of the lift and drag, some remarks are in order regarding the appropriate charging of losses in either the full capture (Fig. 1b) or spillage (Fig. 1a) configurations. Consider first Fig. 1b. Here the inlet may be regarded as encompassing the entire section from A to B and any shock or skin friction losses must be charged correctly to the inlet. The external surfaces of the vehicle thus consist

of the Sections A-C and B-D. This requires, therefore, careful evaluation (or at least wide parametric variations) of the values of r_{in}.

For the balanced configuration since the aerodynamics now require capture at A_a, the inlet extends only from B to F and the shock and boundary layer losses in the region A to B are to be charged to the airframe. This distinction from the full capture geometry also necessitates, then, careful selection for the value of the inlet recovery.

For either configuration we may observe that, in general, but dependent on the geometry, the thrust is not aligned with the drag. Consequently a typical vector diagram for lift, drag and total thrust might appear as in the following sketch

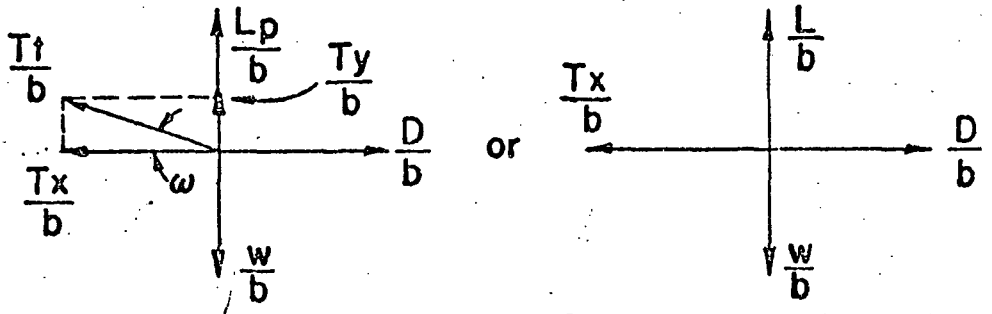

where L_p is the lift due to the pressure forces only, ω the inclination of the thrust and W the weight of the vehicle. There would appear to be two ways of defining an appropriate lift-to-drag ratio, L/D, depending on the interpretation of the total lift force:

(i) Lift is due to pressure force only; then

$$L/D = L_p/D$$

(ii) Lift is due to pressure forces and the component of lift due to the thrust; then

$$L/D = (L_p + T_{total}\sin\omega)/D$$

Both definitions will be used here; the first for the accelerating, full capture configuration, and the second when we need to be sure that a balanced vehicle is obtained as with the spillage geometry.

Now let us turn our attention to the individual components which make up the lift and drag for the two configurations in Fig. 1.

(a) Full capture configuration.

In this configuration, we take the bottom plate to be parallel to the upper plate with leading edge shock from the wedge fully-captured. Note that if the angle of attack α_1, and the wedge angle δ are kept constant, the geometry and the area ratio, A_e/A^*, of the vehicle are determined. With A_e/A^* known, the exit pressure, p_e, is determined from the engine calculations. This will, in general, be higher than the local external flow pressure and the exhaust stream will deflect an angle θ such that pressures are balanced on either side of the slip-stream between the exhaust jet and the local external flow.

Note that in this case, the problem as posed maintains a constant capture area, A_a. Naturally this does not represent a balanced design and no attempt is made to equate the thrust produced by the engine with the drag of the vehicle; this will indicate then, for example, the effects of variations of equivalence ratio for an accelerating vehicle.

Because the analysis is two dimensional, all forces to be computed will be per uniform depth of profile, b. In the ratio of two forces,

such as the lift to drag ratio, this depth drops out, however, since $(L/b) / (D/b) = L/D$.

The drag on the profile consists of the viscous drag and the pressure drag. The viscous drag on all surfaces exposed to the local external flow was calculated assuming a turbulent boundary layer according to Ref. 14:

$$D_{vis}/b = 0.036\ \rho_\infty U_\infty^2\ \ell(R_{e\infty})^{-1/5} \tag{12}$$

The skin friction drag is then composed of components according to

$$D_{vis}/b = [D_{vis}/b]_{AC} + [D_{vis}/b]_{BD} \tag{13}$$

The total drag is given by

$$D/b = D_{vis}/b + \Sigma p_i \sin\alpha_i \text{ (along AC, AB, BD and DE)} \tag{14}$$

The lift due to the pressure forces is obtained from simply:

$$L_p/b = \Sigma p_i \cos\alpha_i \text{ (along AC, AB, BD and DE)} \tag{15}$$

As noted above since we are not interested in a thrust equal drag configuration, it seems reasonable to compute the lift-to-drag ratio according to the first definition above and the total thrust from Eq. (11b).

(b) Configuration with spillage

In this configuration the leading edge shock is allowed to spill and the nozzle is assumed to be designed so that the exit pressure balances the lower flow pressure, i.e. $p_e = p_a$. The stagnation pressure, p_{0a} is then

a function of the angle of attack α_2.

Using the condition $p_e = p_a$ in the engine calculations determines uniquely the area ratio A_e/A^*. The inclination of the top plate is then determined so that this correct exit area is obtained at the end of the configuration. The engine is now located between BCE and hence the skin friction drag along AB must now be included in the total viscous drag. Thus:

$$D_{vis}/b = [D_{vis}/b]_{AB} + [D_{vis}/b]_{FD} + [D_{vis}/b]_{AC} \qquad (16)$$

and the total drag becomes

$$D/b = D_{vis}/b + \Sigma p_i \cos\alpha_i \text{ (along AB, BF, FE, AC)} \qquad (17)$$

The lift due to the pressure forces is then

$$L_p/b = \Sigma p_i \cos\alpha_i \text{ (along AB, BF, FE, AC)} \qquad (18)$$

Here, since we are interested in a balanced configuration and since $\omega=\alpha_2$, the total lift may be determined according to the second of the definitions as:

$$L/b = L_p/b + T_{total} \sin\alpha_2 \qquad (19)$$

with the total thrust given as before in Eq.(11b).

The thrust component needed to balance the drag is simply $T_x=T_{total}\cos\alpha_2$. The thrust can be varied by changing the capture area to control the mass flow through the engine. Thus an iteration on A_a is performed

until T_x=D and when this condition obtains one operating point of the configuration is reached.

3. Results.

We now turn our attention to some of the results obtained from the two configurations considered in Section 2.

A. Full capture.

Consider first the performance of the engine in terms of the fuel specific impulse, $I_{sp}=(T/\dot{m}_f)$. The variation of I_{sp} with angle of attack and equivalence ratio is presented in Fig. 3. For these calculations the leading wedge angle was fixed at 4°; the other parameters selected are indicated on the charts. Note that while the fuel-specific-impulse decreases with equivalence ratio (the fuel added increased at a faster rate than does the thrust) the air specific impulse naturally rises.

The basic results for lift-to-drag ratio, excess thrust-to-drag (T_x-D) and additional thrust-for-lift (L_p-T_y) as functions of equivalence ratio and angle of attack are presented in Figs. 4 and 5 respectively. The parameters selected are indicated on the curves. We observe, in Fig. 4, that, as might be expected, for a fixed mass flow (fixed capture area), as the burning rate increases the excess thrust-to-drag increases rapidly. Because of the requirement of the nozzle expansion and the resulting wave pattern,we also find that the resultant lift-to-drag ratio decreases substantially. However this is nearly offset by a corresponding rise in the thrust-for-lift, T_y/L_p. Indeed as Φ varies from 0.1 to 0.5, L_p/D decreases by roughly 10% while the total lift-to-drag ratio, $(L_p+T_y)/D$ drops only by 3%.

The results corresponding to angle of attack variations (Fig. 5) are interesting in several respects. We first point out that higher angles of attack were excluded from this treatment since it seems unreasonable from other considerations (e.g. heat transfer, sonic boom) to expect larger variation. We observe that due to the nature of the wave pattern in the nozzle the vehicle as designed produces positive thrust at zero angle of attack; the exhaust pressure is extremely high (necessitated by the large mass flows) and so turns the streamline favorably. Also corresponding to the high nozzle exhaust pressure we see that substantial thrust-for-lift is obtained at small angles of attack, indeed here $L_p < T_y$ so that the total L/D is substantially higher then indicated solely by L_p/D. We also note that the lift-to-drag ratio (L_p/D) seems to reach a peak at roughly $\alpha_1 \sim 2^\circ$ and maintains its level to $\alpha_1 \sim 5^\circ$. Finally, the results for L_p/D were investigated for sensitivity to inlet recovery. Admittedly there is some effect although these preliminary estimates indicate that even for r_{in} as low as 0.35 the absolute levels for L_p/D are reasonable.

It is pertinent also to make some remarks here regarding vehicle volume-for-payload variations under these conditions. By keeping the capture area, A_a, and the leading edge wedge angle, δ, fixed the volume of the configuration remained practically constant as the engine parameters were varied according to Figs. 4 and 5. This is necessary and desirable if the volume requirements are known and the vehicle is to be designed around such limitations.

B. Spillage

As discussed before this more interesting configuration is studied to

provide some indication of the variations of performance that can be expected for a balanced (thrust equals drag) vehicle. The captured mass flow is limited by varying the inlet area A_a.

The corresponding variation of fuel specific impulse is presented in Fig. 6 for a fixed vehicle, sized according to AC=400 ft. and FD=60 ft. Again, while I_{sp} decreases with increasing Φ, the air specific impulse is growing. The growth is to be attributed both to increases in the level of the thrust and to the corresponding drop in captured mass required for the balanced configuration. Observe that the specific impulse variation with angle of attack (for a typical set of efficiency factors and burning rate) is non-monotonic. Indeed the I_{sp} reaches a peak at an angle of attack of 4°. Amplification of this optimum performance is presented below.

The variation of L/D and capture area (per unit depth) with equivalence ratio are presented in Figs. 7 and 8 respectively. In general as Φ increases the lift-to-drag ratio increases (as before) and since the total thrust is increasing the requisite capture area decreases substantially. This implies then a very thin profile for high L/D with consequently little volume left for payload. This is because the engine is truly integral with the airframe profile (for fixed geometry) and then as the burning rate increases the engine mass flow must decrease to balance the drag.

Variations with angle of attack are presented in Fig. 9, again for fixed geometry, and one typical set of efficiency factors and burning rate. The interesting feature here is that the lift-to-drag ratio reaches a maximum at an angle of attack of 4°. We further observe that the capture area is a monotonically increasing function of angle of attack growing substantially due to the attendant drag increases. Again, here the angle of

attack variations are limited due to the considerations mentioned above. The indicated behavior of these results imply a tradeoff between high L/D and sufficient volume for payload. In conjunction with these volume considerations we may note parenthetically that each operating point of these figures corresponds to a different vehicle since for convenience the dimensions of the airframe, AC and FD,were held constant.

Finally consideration of the sensitivity of the results are presented in Table 1. Here for a fixed angle of attack are variations of L/D and capture area for small variations in inlet recovery, nozzle efficiency and equivalence ratio as derived from the data. Note that only small variations obtain for substantial changes in r_{in} and η_n which lead to reasonable confidence in the trends indicated in Figs. 7-9.

4. Final Remarks.

We have presented a preliminary study of an integrated engine-airframe hypersonic vehicle operating at Mach 6. Indications are that reasonable lift-to-drag ratios may be obtained with either an accelerating or cruise configuration. The final questions remaining are related to the basis applicability of this two dimensional analysis to a more realistic three dimensional geometry and to the actual performance of the vehicle, including e.g. pitching movements, etc.

Consider then a typical design such as presented in Fig. 10. We indicate only the bottom surface of a three dimensional integrated engine-airplane. Note that the engine compartments are similar in nature to the two

dimensional flow field of Fig. 1. Indeed appropriate aerodynamic considerations indicate that the flow field which the engine sees is truly two dimensional. The entire region will appear to be a combination of the preceding configurations embracing features of the spillage geometry and incomplete expansion in the nozzle. As before, we may employ scheduling of the fuel-air ratio to control here the nozzle exhaust wave patterns and thereby control e.g. lift-to-drag ratio and resultant pitching movements. Thus the applicability of these results may be much broader than what appears at first glance.

References

1. Newbauer, John, Ed., "Case for the Hypersonic Transport", Aeronautics and Astronautics, October 1966.
2. Ferri, A., "Possible Direction of Future Research in Air Breathing Engines", 4th AGARD Colloguium of High Mach Number Airbreathing Engines, Milan, Italy, April 1960.
3. Sedden, J., "Comment on 'Some Considerations of Hypersonic Inlets'", 4th AGARD Colloquium of High Mach Numbers Airbreathing Engines, Milan, Italy, April 1960.
4. McConarty, W.A., and Anthony, F.M., "Design and Evaluation of Active Cooling Systems for Mach 6 Cruise Vehicle Wings", Bell Aerosystem Company, Report No. 7305-901001.
5. Parthasarathy, K. and Zakkay, V., "An Experimental Investigation of Turbulent Slot Integration at Mach 6", submitted to the AIAA J.
6. Hoydysh, W., Fox, H., and Ferri, A., "Performance and Design of a Turbocooler", to be issued as a New York University report.
7. Fox, H., Cronin, R. and Hoydysh, W., "Application of the Rankine Cycle to Cooling of Hypersonic Aircraft", New York University Aerospace Laboratory, Report No. 69-13 (1969).
8. Ferri, A. and Fox, H., "Analysis of Fluid Dynamics of Supersonic combustion Processes Controlled by Mixing", paper presented at the 12th Symposium (International) on Combustion, The Combustion Institute, Potiers, France, July, 1968.
9. Agnone, A., "Design and Theoretical Performance of a two dimensional Scramjet Engine Utilizing Thermal Compression in the Inlet", New York University Aerospace Laboratory, Report No. 69-14 (1969).

10. Ferri, A., "Review of Scramjet Propulsion Technology, J. of Aircraft 5,1, 3-10. Jan.-Feb. 1968.

11. Hesse, W.J. and Munford, W.V.S., Jr., "Jet Propulsion for Aerospace Application", 2nd Edition Pitman Publishing Company, New York (1964).

12. Anon. "Combustion Charts for Hydrocarbon Fuels", Pratt and Whitney Aircraft Co., Hartford, Connecticut.

13. Shapiro, A., "The Dynamics and Thermodynamics of Compressible Fluid Flow", Vol. 1, Ronald Press, New York, (1958).

14. Schlichting, H., "Boundary Layer Theory", 6th Edition, McGraw-Hill Book Company, New York (1968).

TABLE I

Variation of Parameters for Balanced Configuration with Spillage

A. Effect of r_{in} : $\Phi = 0.3$ $\eta_n = 0.9$ $\alpha = 8^\circ$

r_{in}	L/D	A_a/b
0.3	5.94	10.0 ft.
0.5	6.06	8.5 ft.

B. Effect of η_n : $\Phi = 0.3$ $r_{in} = 0.3$ $\alpha = 8^\circ$

η_n	L/D	A_a/b
0.90	5.94	10.0 ft.
0.94	6.05	7.0 ft.
0.98	6.10	6.4 ft.

C. Effect of Φ : $\eta_n = 0.9$ $r_{in} = 0.3$ $\alpha = 8^\circ$

Φ	L/D	A_a/b
0.1	5.43	23.0 ft.
0.3	5.94	10.0 ft.
0.5	5.98	6.4 ft.

LIST OF FIGURES

a) ENGINE - SCHEMATIC

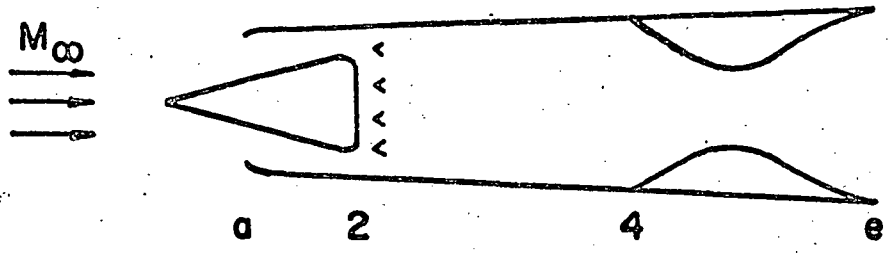

b) FULL CAPTURE CONFIGURATION

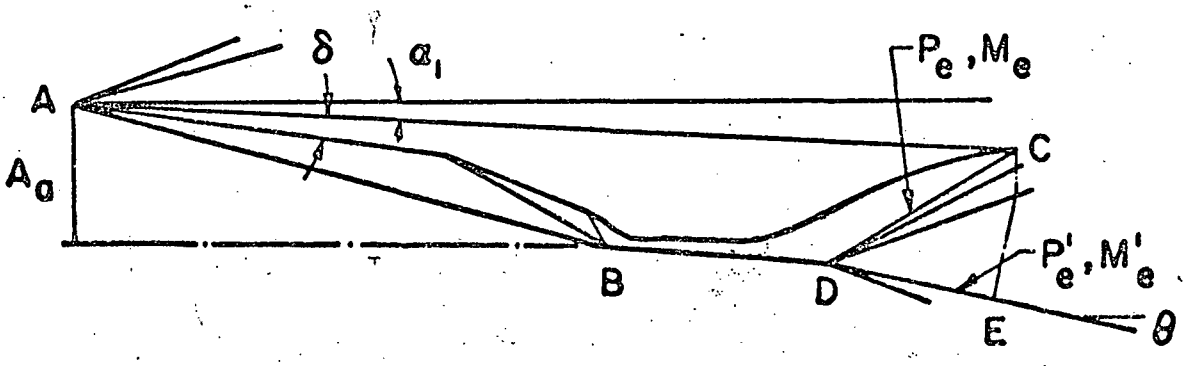

c) SPILLAGE CONFIGURATION

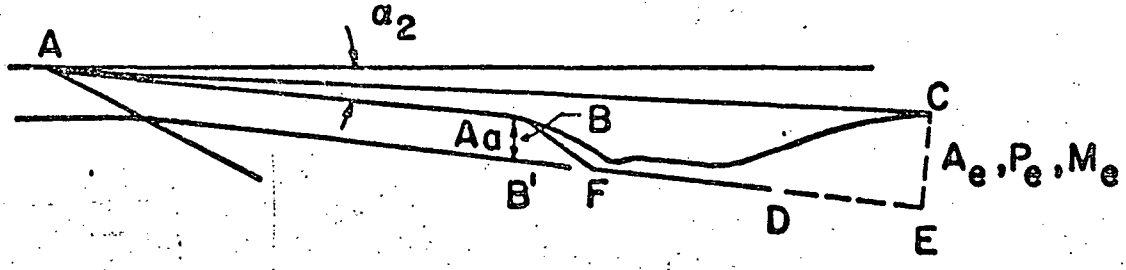

FIG. 1

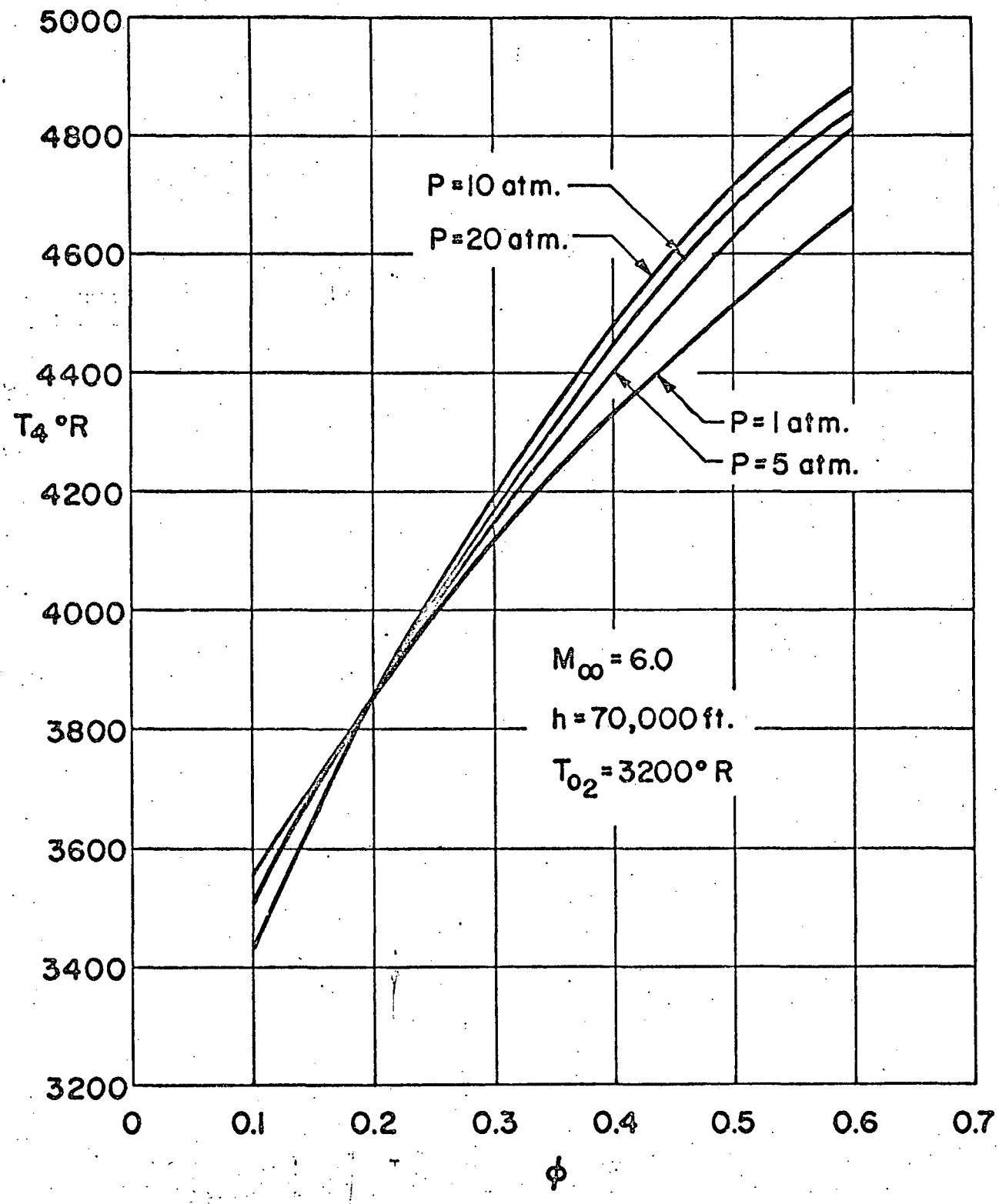
5000
4800
4600
4400
4200
4000
3800
3600
3400
3200
T_4 °R
P = 10 atm.
P = 20 atm.
P = 1 atm.
P = 5 atm.
$M_\infty = 6.0$
h = 70,000 ft.
$T_{o_2} = 3200°$ R
0
0.1
0.2
0.3
0.4
0.5
0.6
0.7
ϕ

FIG. 2

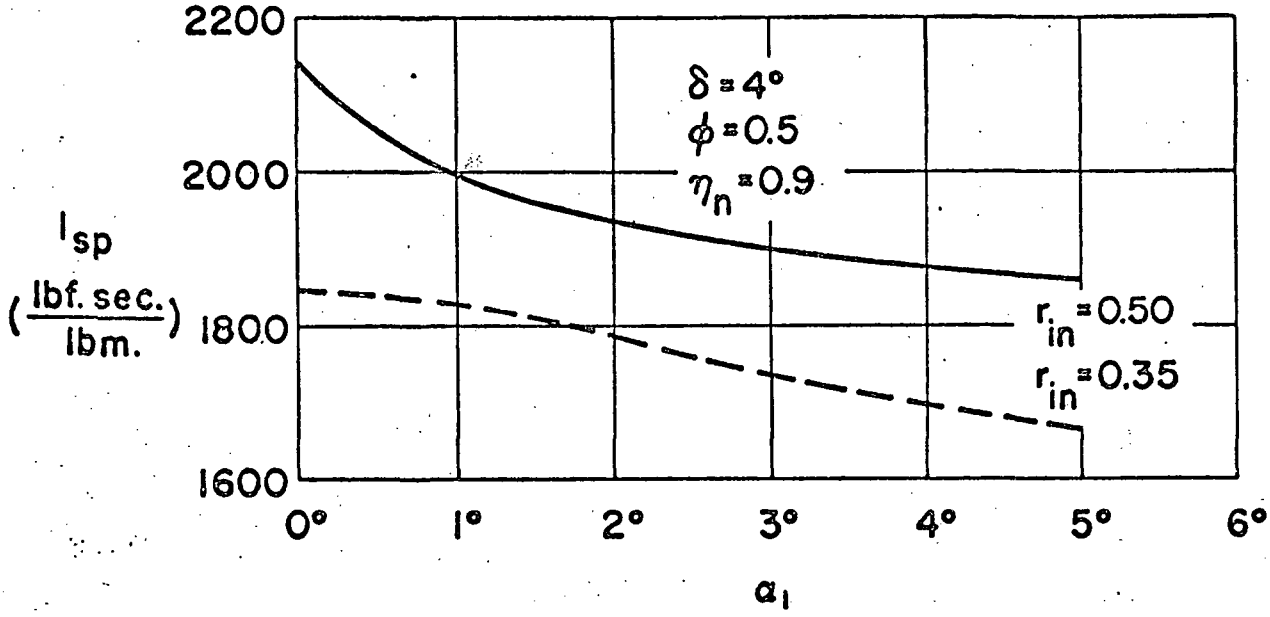

a) EFFECT OF ANGLE OF ATTACK

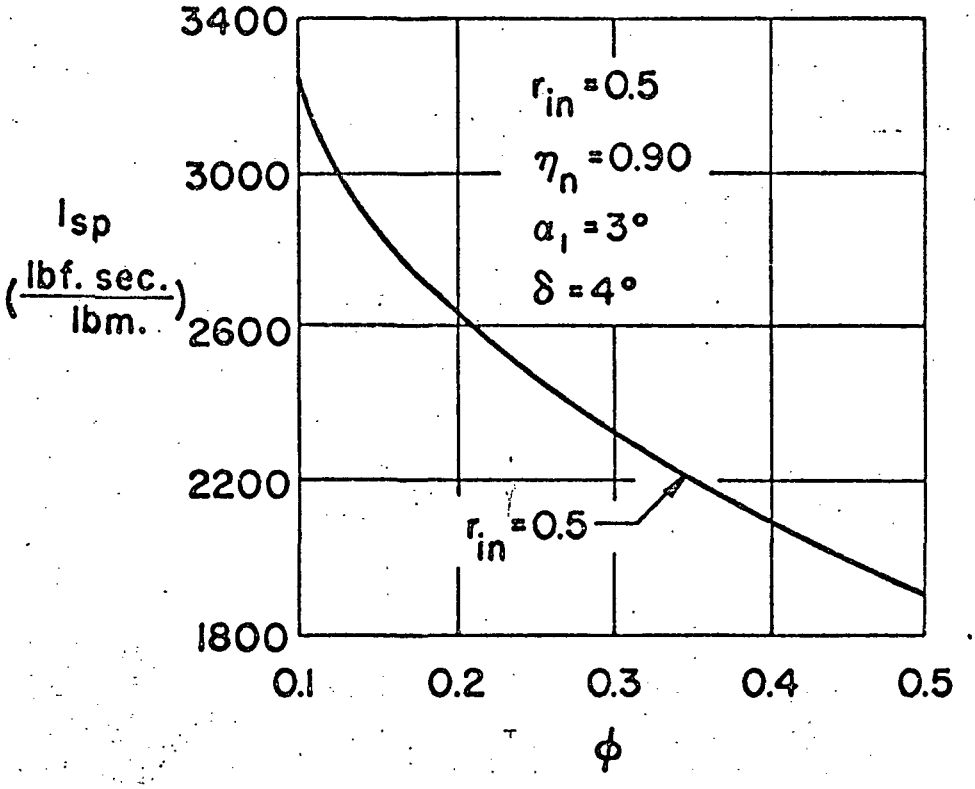

b) EFFECT OF EQUIVALENCE RATIO

FIG. 3

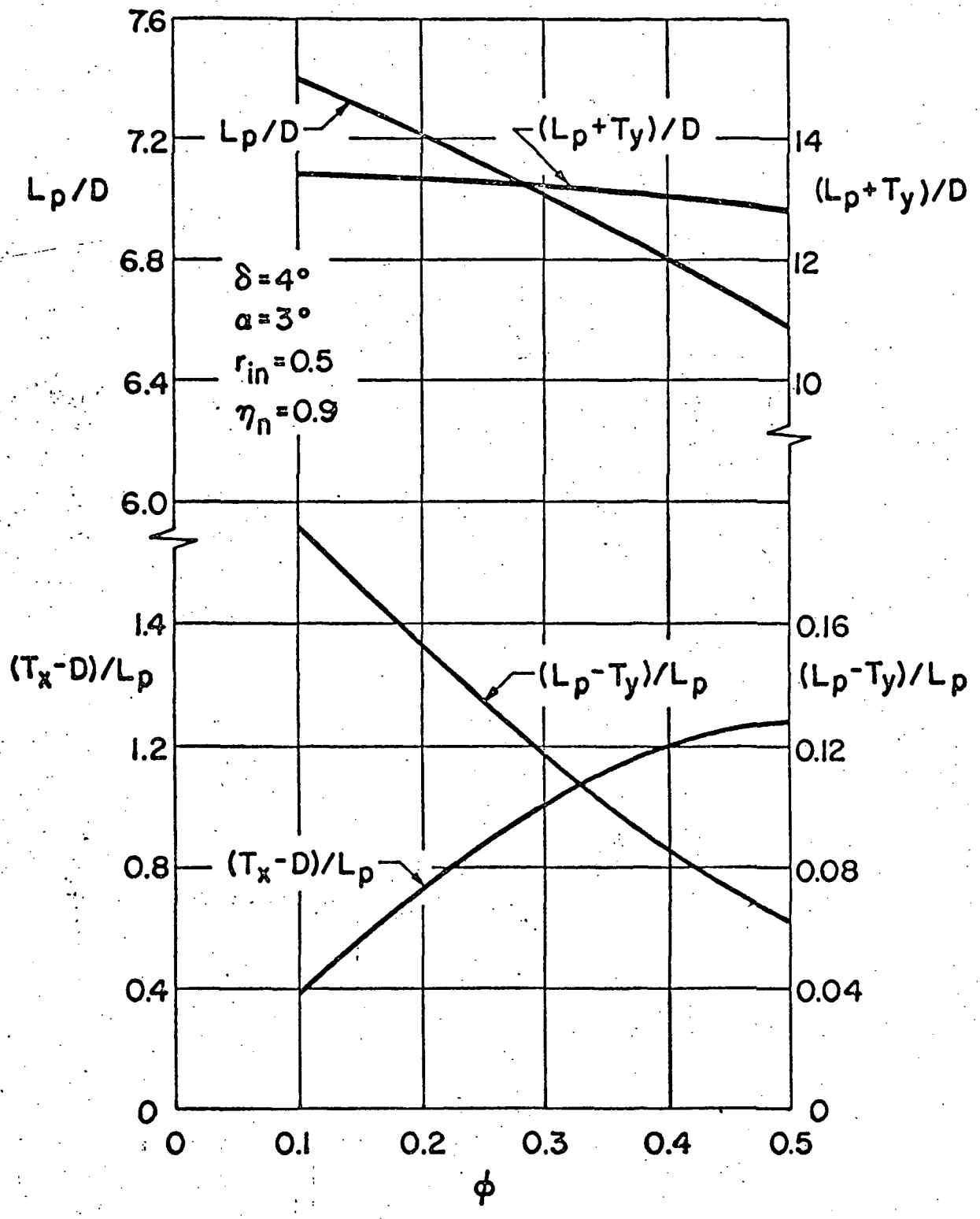
7.6
7.2
6.8
6.4
6.0
1.4
1.2
0.8
0.4
0
L_p/D
$(T_x-D)/L_p$
L_p/D
$(L_p+T_y)/D$
$\delta=4°$
$\alpha=3°$
$r_{in}=0.5$
$\eta_n=0.9$
$(L_p-T_y)/L_p$
$(T_x-D)/L_p$
14
12
10
0.16
0.12
0.08
0.04
0
$(L_p+T_y)/D$
$(L_p-T_y)/L_p$
0
0.1
0.2
0.3
0.4
0.5
ϕ

FIG. 4

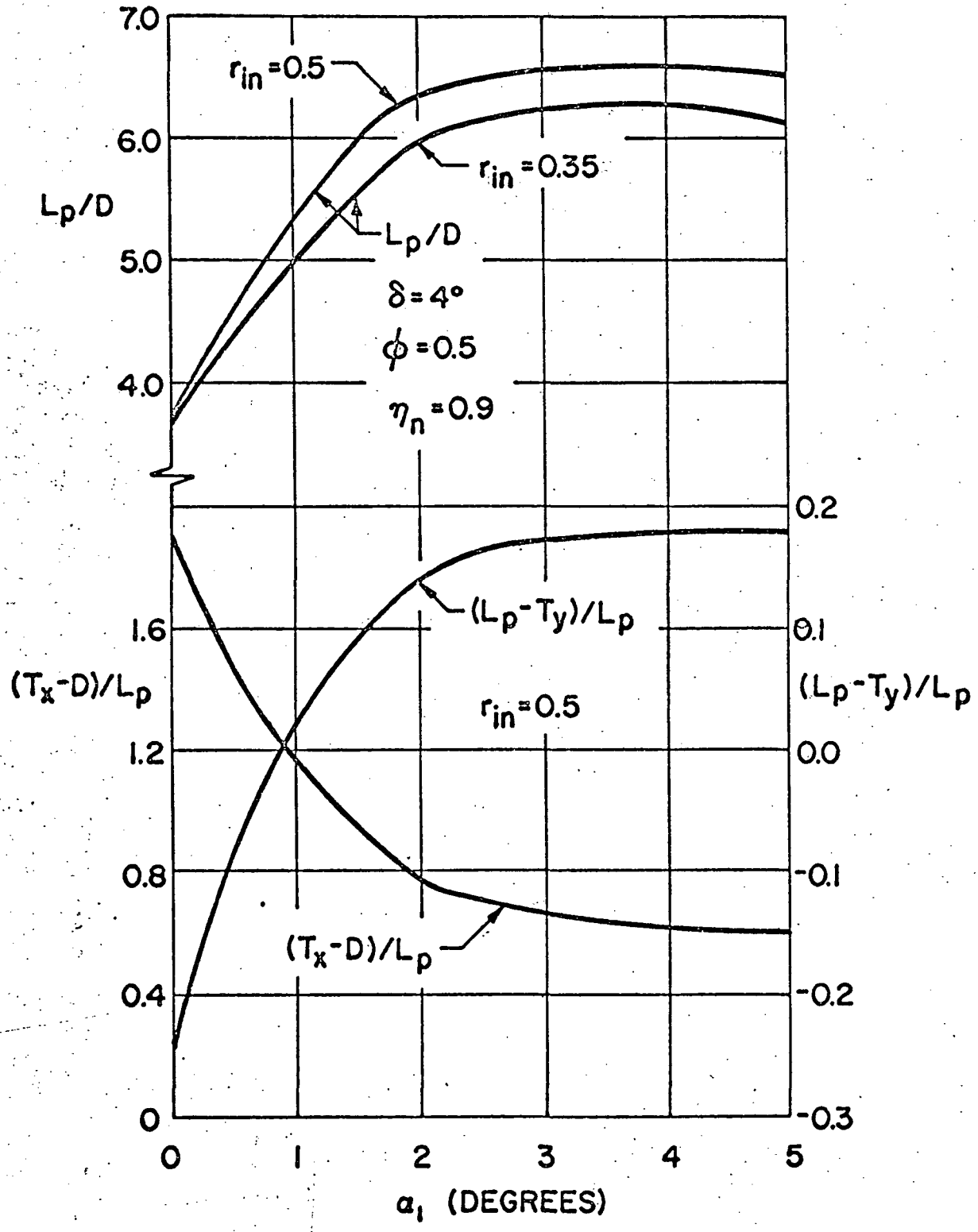
7.0
6.0
5.0
4.0
1.6
1.2
0.8
0.4
0
L_p/D
$r_{in}=0.5$
$r_{in}=0.35$
L_p/D
$\delta=4°$
$\phi=0.5$
$\eta_n=0.9$
$(T_x-D)/L_p$
$(L_p-T_y)/L_p$
$r_{in}=0.5$
$(T_x-D)/L_p$
0.2
0.1
0.0
-0.1
-0.2
-0.3
$(L_p-T_y)/L_p$
0
1
2
3
4
5
α_i (DEGREES)

FIG. 5

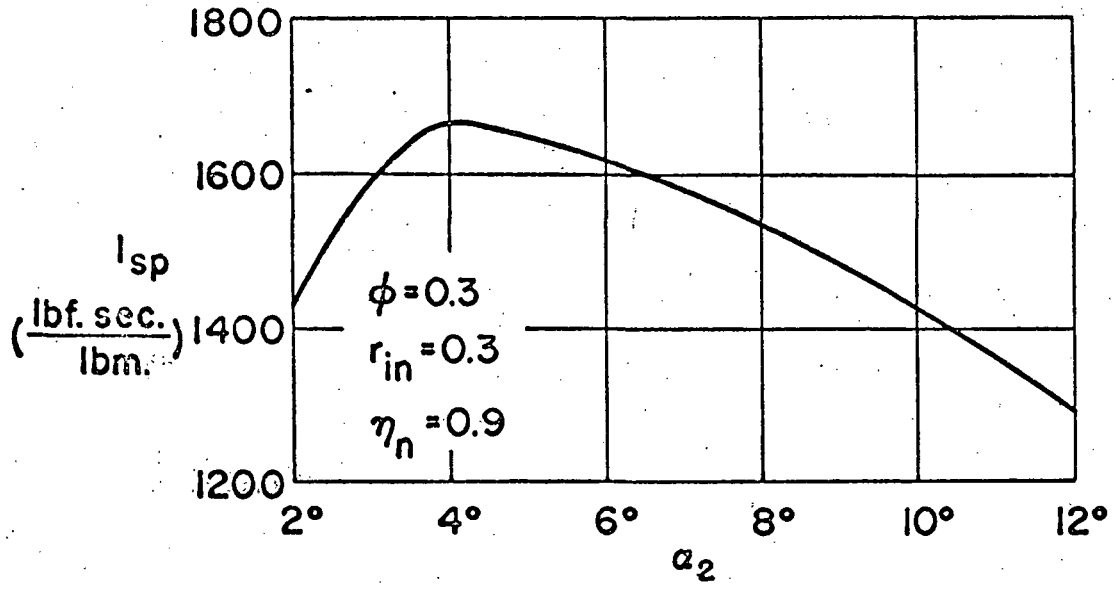

a) EFFECT OF ANGLE OF ATTACK

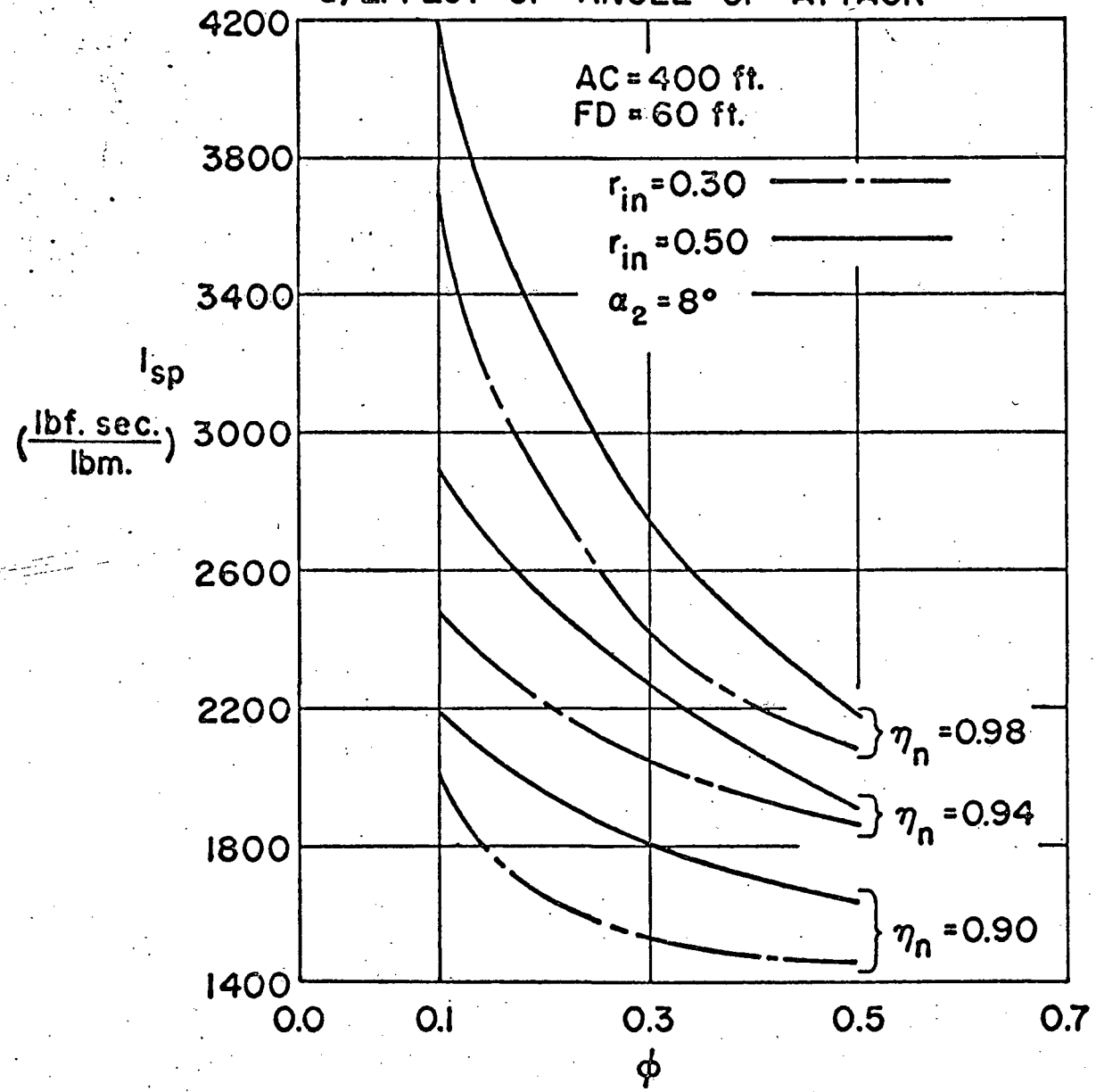

b) EFFECT OF EQUIVALENCE RATIO

FIG. 6

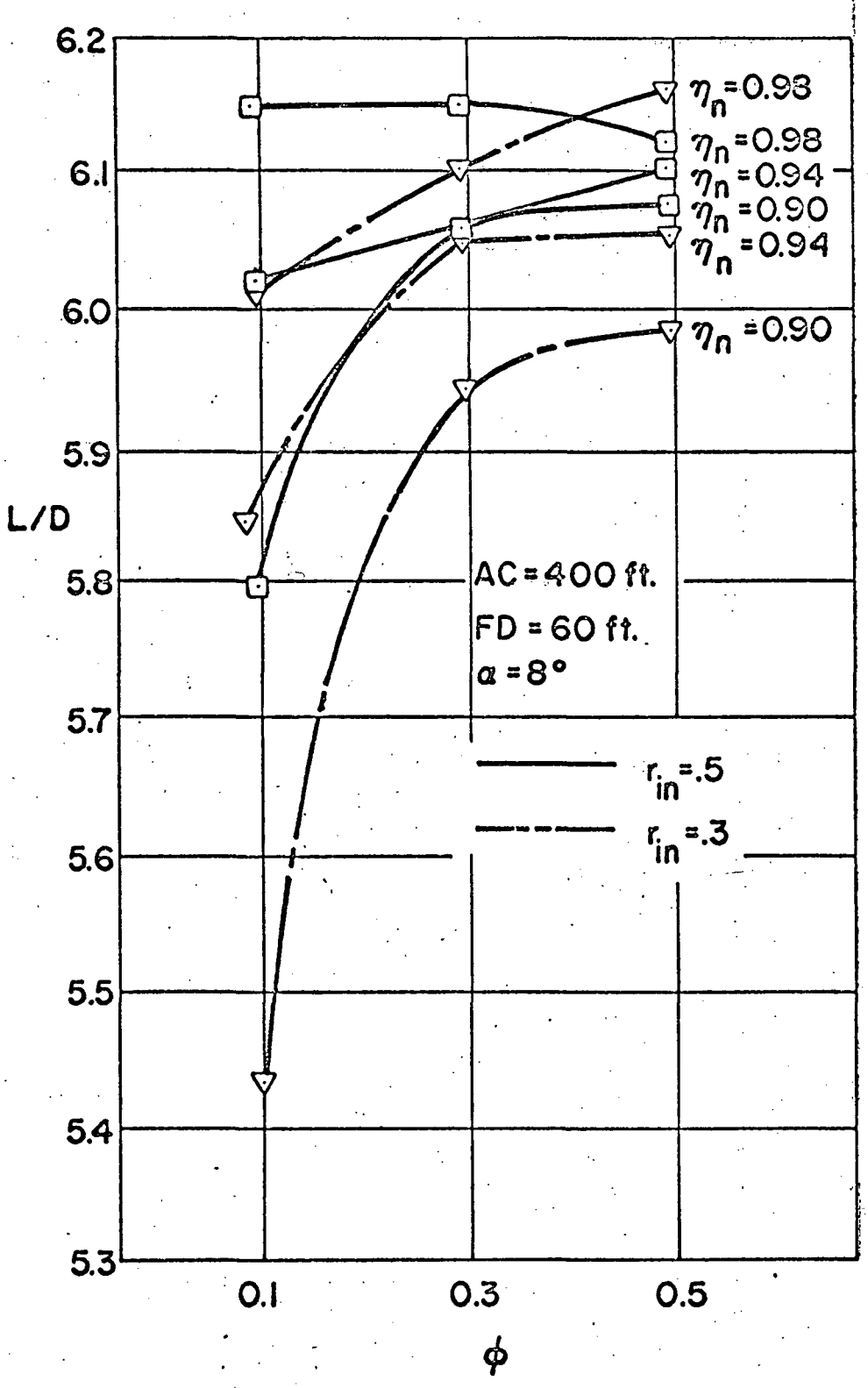
6.2
6.1
6.0
5.9
5.8
5.7
5.6
5.5
5.4
5.3
L/D
0.1
0.3
0.5
ϕ
η_n=0.93
η_n=0.98
η_n=0.94
η_n=0.90
η_n=0.94
η_n=0.90
AC=400 ft.
FD=60 ft.
α=8°
r_{in}=.5
r_{in}=.3

FIG. 7

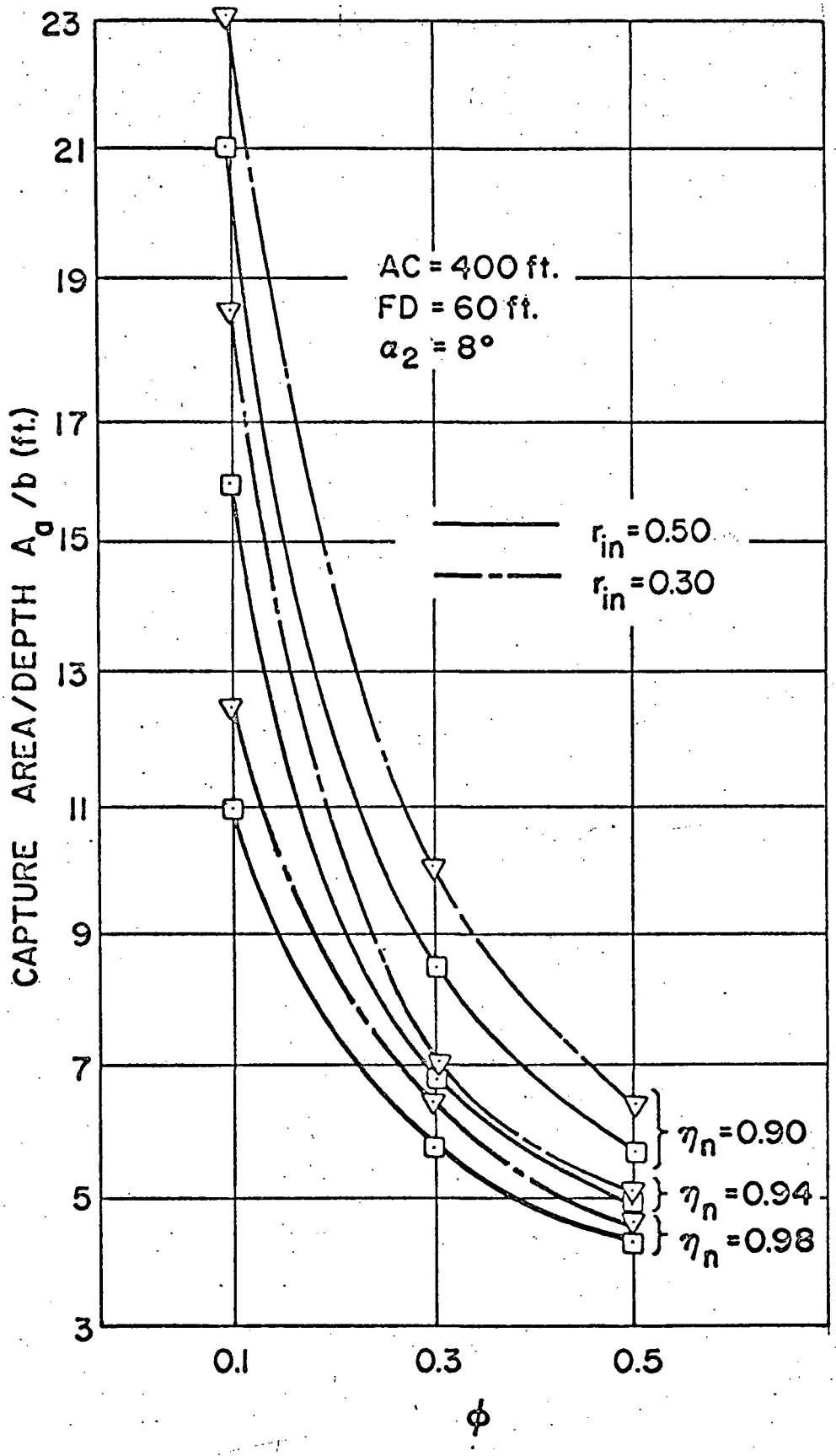
AC = 400 ft.
FD = 60 ft.
a_2 = 8°
r_{in} = 0.50
r_{in} = 0.30
η_n = 0.90
η_n = 0.94
η_n = 0.98
CAPTURE AREA/DEPTH A_a/b (ft.)
23
21
19
17
15
13
11
9
7
5
3
0.1
0.3
0.5
ϕ

FIG. 8

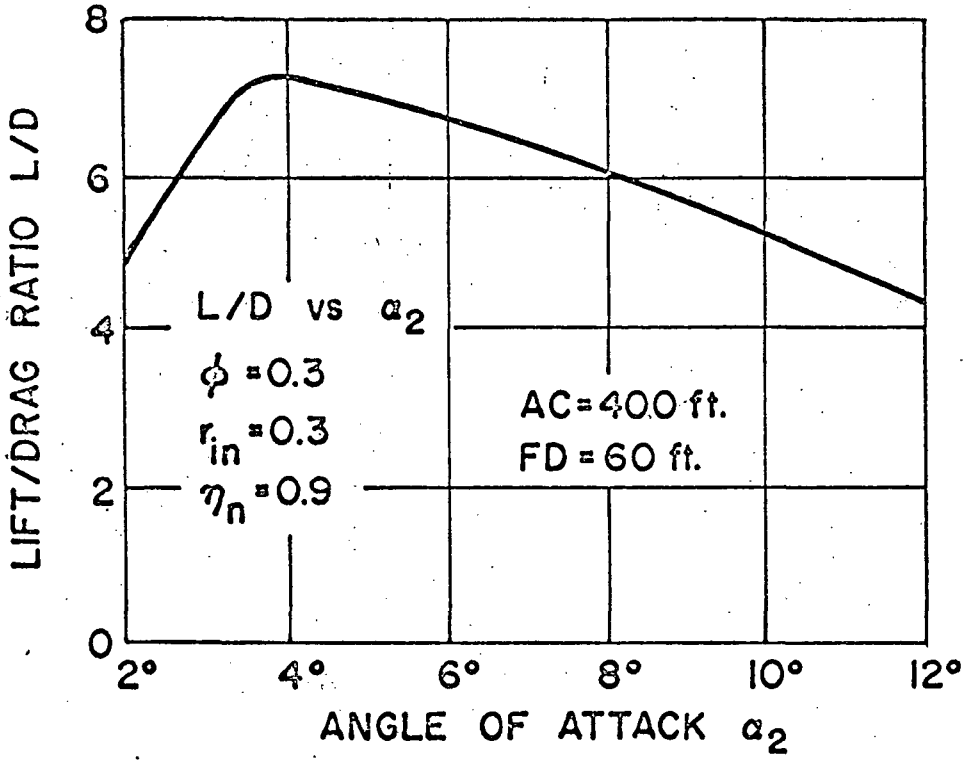
LIFT/DRAG RATIO L/D
8
6
4
2
0
L/D vs α_2
ϕ = 0.3
r_{in} = 0.3
η_n = 0.9
AC = 400 ft.
FD = 60 ft.
2°
4°
6°
8°
10°
12°
ANGLE OF ATTACK α_2

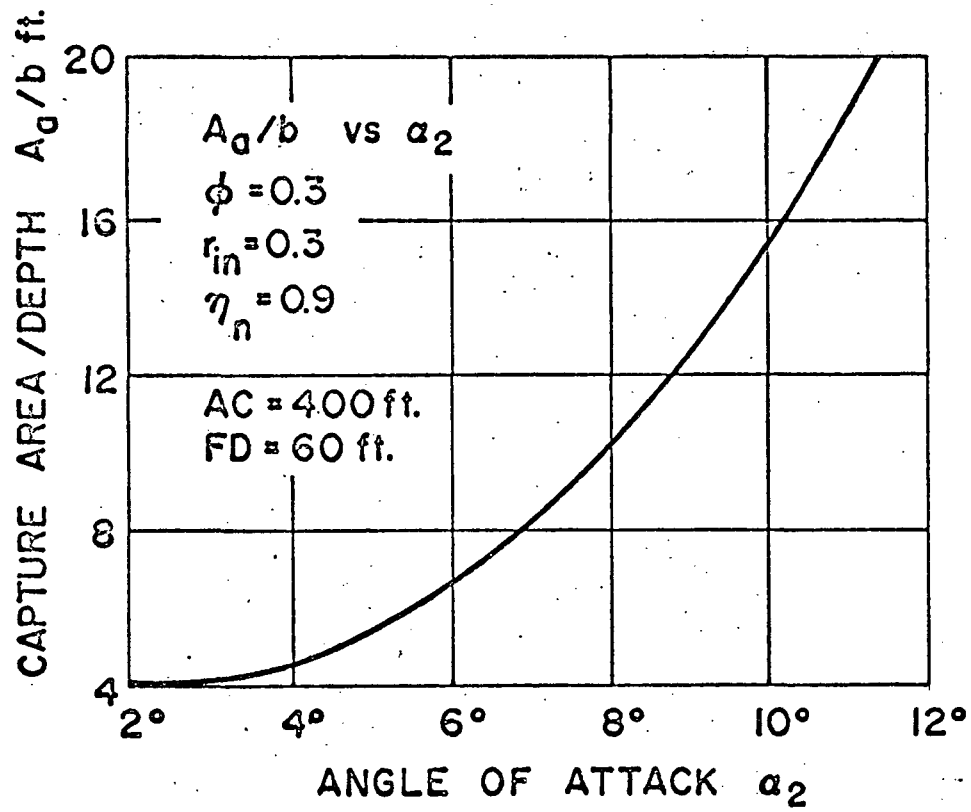
CAPTURE AREA /DEPTH A_a/b ft.
20
16
12
8
4
A_a/b vs α_2
ϕ = 0.3
r_{in} = 0.3
η_n = 0.9
AC = 400 ft.
FD = 60 ft.
2°
4°
6°
8°
10°
12°
ANGLE OF ATTACK α_2

FIG. 9

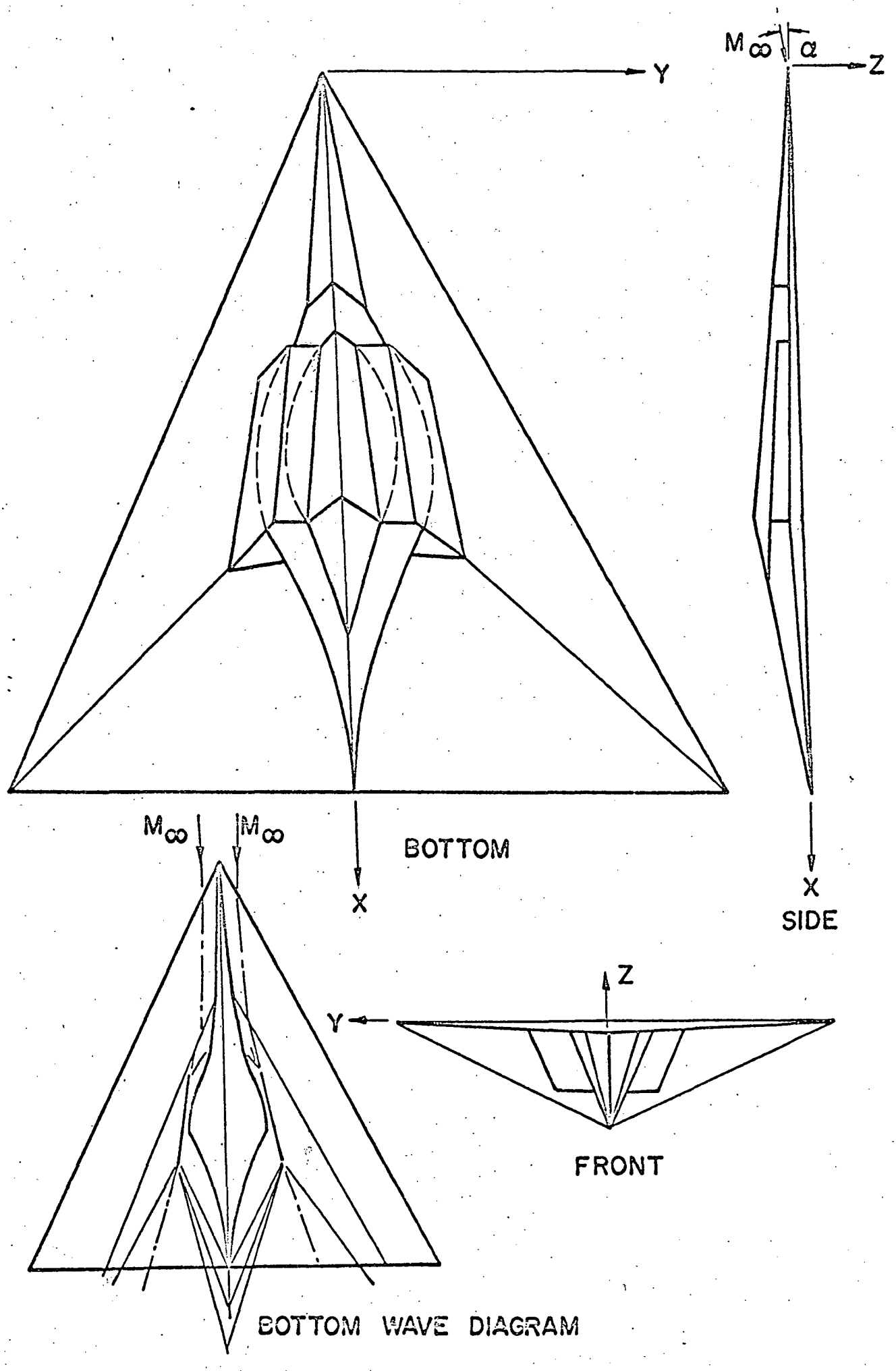

FIG. 10